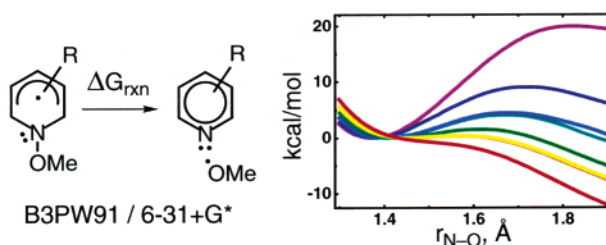# JOC Article

Density Functional Theory Predicts the Barriers for Radical Fragmentation in Solution

Edward D. Lorance, Kirstin Hendrickson, and Ian R. Gould*

Department of Chemistry and Biochemistry, Arizona State University, Tempe, Arizona 85287-1604

igould@asu.edu

N-Methoxypyridyl radicals formed by one-electron reduction of the corresponding cationic hetero-cycles undergo N−O bond cleavage. Experimental activation free energies for a series of these bond fragmentations are compared to corresponding barriers determined from electronic structure calculations. The DFT barriers agree well with those from experiment, being smaller than the latter values by an average value of ca. 1 kcal/mol, for rate constants varying over almost 3 orders of magnitude, or within ca. 3 kcal/mol over 8 orders of magnitude of rate constant. For a model compound, the B3PW91/6-31+G* hybrid density functional method is also found to be in good agreement with the MCSCF-MRMP2 method. One of the reactions is found by DFT to have no minimum for the reactant radical, consistent with a truly barrierless reaction.

Introduction

Density functional theory (DFT) methods for electronic structure calculations have found wide-ranging applications in qualitative and quantitative descriptions of organic chemical reactions,[1] particularly in problems related to open-shell systems,[2] which are traditionally difficult to describe properly using Hartree−Fock (HF) methods.[3] Direct comparison of DFT with accurate ab initio methods has provided several examples in which the two approaches give similar results, although the fundamental reason for the agreement may not always be exactly clear.[3] A weakness of DFT methods is a lack of logical higher levels of computation which could be used to improve the calculations, analogous to the MP*n* series in perturbation theory. The obvious strength of DFT is its apparent ability to properly handle large and complex systems that are difficult or impossible using other computational methods. DFT has been found to provide accurate structures, thermochemical data, and in several cases, reaction barriers that are close to those from accurate ab initio methods.[2,4]

Less common are direct comparisons of DFT with reaction kinetics and barriers, and examples in which DFT calculations are directly compared to experimental rate data for open-shell systems in solution are rare.[2] This is unfortunate, since demonstration of the successful description of complex reactions in solution would seem to be an obvious goal in the development of DFT. Such a direct comparison of DFT and experiment for an open-

(1) (a) Hohenberg, P.; Kohn, W. *Phys. Rev.* **1964**, *136*, B864. (b) Perdew, J. P.; Chevary, J. A.; Vosko, S. H.; Jackson, K. A.; Pederson, M. R.; Singh, D. J.; Fiolhais, C. *Phys. Rev. B* **1992**, *46*, 6671. (c) Ziegler, T. *Chem. Rev.* **1991**, *91*, 651. (d) *Density Functional Methods in Chemistry*; Labanowski, J., Andzelm, J., Eds.; Springer: Berlin, 1991. (e) Becke, A. D. *J. Chem. Phys.* **1993**, *98*, 5648. (f) Bickelhaupt, F. M.; Baerends, E. J. *Rev. Comput. Chem.* **2000**, *15*, 1.

(2) (a) Cramer, C. J.; Dulles, F. J.; Storer, J. W.; Worthington, S. E. *Chem. Phys. Lett.* **1994**, *218*, 387. (b) Wiest, O. *THEOCHEM* **1996**, *368*, 39. (c) BelBruno, J. J. *J. Chem. Soc., Faraday Trans.* **1998**, *94*, 1555. (d) Bally, T.; Borden, W. T. *Rev. Comput. Chem*. **1999**, *13*, 1. (e) Romano, R. M.; Della Vedova, C. O.; Boese, R.; Hildebrandt, P. *Phys. Chem. Chem. Phys*. **1999**, *1*, 2551. (f) Ihee, H.; Kua, J.; Goddard, W. A., III; Zewail, A. H. *J. Phys. Chem. A* **2001**, *105*, 3623. (g) Ihee, H.; Zewail, A. H.; Goddard, W. A., III. *J. Phys. Chem. A* **1999**, *103*, 6638. (h) Karady, S.; Cummins, J. M.; Dannenberg, J. J.; del Rio, E.; Dormer, P. G.; Marcune, B. F.; Reamer, R. A.; Sordo, T. L. *Org. Lett.* **2003**, *5*, 1175.

(3) (a) Pople, J. A.; Gill, P. M. W.; Handy, N. C. *Int. J. Quantum Chem.* **1995**, *56*, 303. (b) Jensen, F. *Introduction to Computational Chemistry*; Wiley: New York, 1999; pp 189, 274. (c) Wittbrodt, J. M.; Schlegel, H. B. *J. Chem. Phys.* **1996**, *105*, 6574.

shell organic reaction in solution is the subject of the present work.

The reaction chosen for study involves exothermic N—O bond cleavage in a series of *N*-methoxypyridyl radicals, the kinetics of which have been studied in our laboratory over a wide range of rates and barriers.[5] DFT calculations using the B3PW91 hybrid density functional method are compared to CASSCF for a model compound, and DFT and experimental reaction free energies are compared. The results demonstrate good agreement of the DFT barriers for reaction with those from CASSCF calculations and with experiment.

Results and Discussion

Overview of the Reaction. The reaction under study is exothermic N—O bond fragmentation in the radicals formed upon one-electron reduction of *N*-methoxyheterocycles, as illustrated for the parent heterocycle *N*-methoxypyridinium in eq 1. The rate constants, k_{fr}, for
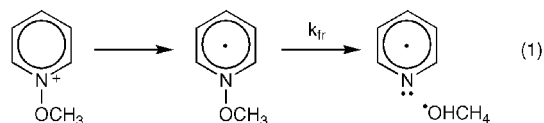
these reactions have been described in previous publications.[5] These articles also contain a qualitative theoretical description of the reaction. The initial product of reduction is an *N*-alkoxypyridinyl radical. If the radical was planar, the extra electron would reside in the lowest π^* orbital of the aromatic system. However, the reactive radical is one in which the extra electron is in an orbital with significant N—O σ^* character. Reaction thus requires mixing of pyridinyl π^* and σ^* radicals, which in turn requires bending of the N—O bond out of the plane of the ring via pyramidalization at nitrogen.[5] This feature is common to many bond-breaking reactions in which the ring symmetry plane must be broken to allow the mixing of the otherwise orthogonal σ and π systems.[6,7] Bond stretching in the absence of pyramidalization does not allow mixing of the π^* and σ^* radical configurations and results in a conical intersection, which represents the highest energy point on the ground-state reaction surface.[5a,7] This situation is clearly illustrated in the recent work by Hynes et al. on the related fragmentation of aryl halide radical anions,[7] in particular see Figure 4 in ref 7b. A multiconfigurational theoretical method such

as CASSCF is usually used for reactions involving mixed electronic states.[8] We sought an accurate theoretical description of the radical fragmentation reaction and were interested in performing calculations on the same molecules that were studied experimentally in solution (i.e., not just simple model compounds). Most of these structures, however, proved to be too large for study using CASSCF. For this reason, we investigated the use of DFT calculations and have found that the B3PW91 method gave good results.

Computational Methods and Preliminary Studies on a Model Compound. Initial work concentrated on the simplest possible model of the pyridyl systems, i.e., *N*-hydroxyformamidinium. One-electron reduction of this compound gives the radical **1**, which undergoes N—O bond fragmentation to yield a hydroxy radical and an imine, eq 2. Even though the model does not include all aspects of the pyridyl radical reactions, for example, the radical center on carbon is not delocalized, it does include the most important features of the reactions studied experimentally. Calculations were performed as constrained geometry optimizations at regular N—O bond length intervals, in addition to unconstrained optimizations of the radical minima and reaction transition states. In all cases, the minima and transition states were additionally characterized by post-optimization frequency calculations.
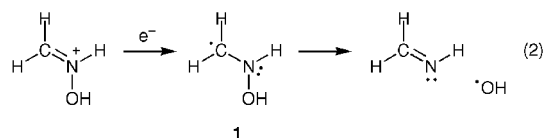
For the multiconfigurational study, the GAMESS full optimized reaction space (FORS) MCSCF method was used, which is identical to CASSCF.[9] An all-electron active space (25 electrons in 15 active orbitals; CASSCF-(25/15)) was used,[10] with multireference Møller—Plessett single-point energy corrections at the minimum and transition state, using the MCQDPT2 method as implemented in GAMESS.[11] The frequencies at these two points on the potential energy surface were computed at the CASSCF level. The 6-31+G* basis set was used.[12]

(4) See, for example: (a) Jensen, F. *Introduction to Computational Chemistry*; Wiley: New York, 1999; Chapters 6 and 11. (b) Jursic, B. S. *THEOCHEM* **1997**, *417*, 89. (c) Kautz, I.; Koch, T.; Malsch, K.; Hohlneicher, G. *THEOCHEM* **1997**, *416*, 223. (d) Lee, T. J.; Rice, J. E.; Scuseria, G. E.; Schaefer, H. F., III. *Theor. Chim. Acta* **1989**, *75*, 81. (e) Scuseria, G. E. *J. Chem. Phys.* **1991**, *94*, 442. (f) Burk, P.; Koppel, I. A.; Koppel, I.; Leito, I.; Travnikova, O. *Chem. Phys. Lett.* **2000**, *323*, 482. (g) Li, J. L.; Brill, T. B. *J. Phys. Chem. B* **2002**, *106*, 9491.

(5) (a) Lorance, E. D.; Kramer, W. H.; Gould, I. R. *J. Am. Chem. Soc.* **2002**, *124*, 15225. (b) Lorance, E. D.; Kramer, W. H.; Gould, I. R. *J. Am. Chem. Soc.* **2004**, *126*, 14071.

(6) (a) Pearson, R. G. *Symmetry Rules for Chemical Reactions*; Wiley: New York, 1976, Chapter 5. (b) Michl, J.; Bonacic-Koutecky, V. *Electronic Aspects of Organic Photochemistry*; Wiley-Interscience: New York, 1990. (c) Salem, L. *Electrons in Chemical Reactions*; Wiley-Interscience: New York, 1982.

(7) (a) Laage, D.; Burghardt, I.; Sommerfeld, T.; Hynes, J. T. *ChemPhysChem* **2003**, *4*, 61. (b) Laage, D.; Burghardt, I.; Sommerfeld, T.; Hynes, J. T. *J. Phys. Chem. A* **2003**, *107*, 11271. (c) Burghardt, I.; Laage, D.; Hynes, J. T. *J. Phys. Chem. A* **2003**, *107*, 11292.

(8) See, for example: (a) Matsunaga, N.; Yarkony, D. R. *J. Chem. Phys.* **1997**, *107*, 7825. (b) Bearpark, M. J.; Robb, M. A.; Yamamoto, N. *Spectrochim. Acta Part A* **1999**, *55*, 639. (c) Blancafort, L.; Adam, W.; Gonzalez, D.; Olivucci, M.; Vreven, T.; Robb, M. A. *J. Am. Chem. Soc.* **1999**, *121*, 10583. (d) Diau, E. W.-G.; De Feyter, S.; Zewail, A. H. *Chem. Phys. Lett.* **1999**, *304*, 134. (e) Robb, M. A.; Olivucci, M. *J. Photochem. Photobiol. A* **2001**, *144*, 237. (f) Quenneville, J.; Ben-Nun, M.; Martínez, T. J. *J. Photochem. Photobiol. A* **2001**, *144*, 229. (g) Klessinger, M. *J. Photochem. Photobiol. A* **2001**, *144*, 217. (h) Blancafort, L.; Jolibois, F.; Olivucci, M.; Robb, M. A. *J. Am. Chem. Soc.* **2001**, *123*, 722.

(9) Schmidt, M. W.; Baldridge, K. K.; Boatz, J. A.; Elbert, S. T.; Gordon, M. S.; Jensen, J. H.; Koseki, S.; Matsunaga, N.; Nguyen, K. A.; Su, S. J.; Windus, T. L.; Dupuis, M.; Montgomery, A. *J. Comput. Chem.* **1993**, *14*, 1347.

(10) It was not originally intended that the active space be as exhaustive; however, critical orbitals were swapped (by GAMESS) for core orbitals during optimization when the model compound was near the transition state, presumably at the point of maximum multireference contribution. It was found that the natural and optimized orbital set, as well as the disposition of the electrons, was altered toward nonsensical results if this swapping was ignored, so the active space was expanded to retain the critical orbitals.

(11) (a) Nakano, H. *J. Chem. Phys.* **1993**, *99*, 7983. (b) Nakano, H. *Chem. Phys. Lett.* **1993**, *207*, 372.

SCHEME 1
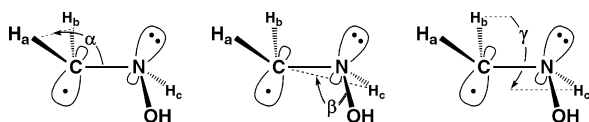
We expect that MCSCF calculations of the FORS type should be capable of accurately describing the reaction coordinate for the reaction of this model.

A minimum was located for **1**, which was found to be pyramidalized strongly at both the nitrogen and carbon atoms, eq 3.[13] The pyramidalization is in opposite direc-

$$(3)$$
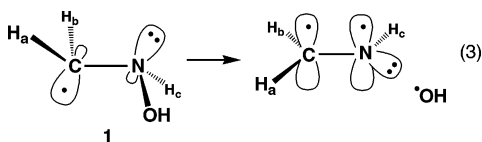
tions, Scheme 1. Pyramidalization at carbon can be characterized by the angle of the nitrogen with respect to the H_a-C-H_b plane (α, Scheme 1). Pyramidalization at nitrogen is required to allow mixing of the π^* and σ^* states and can be characterized by the angle between the oxygen and the $C-N-H_c$ plane (β, Scheme 1). The $H_b-C-N-H_c$ dihedral angle (γ, Scheme 1) gives an indirect measure of both pyramidalizations. As the $N-O$ bond is stretched, the carbon and nitrogen become more planar, as illustrated in Figure 1. Clearly, the carbon becomes sp^2 hybridized as the reaction proceeds, a process that is close to completion by the time the transition state is reached. Hybridization at nitrogen is more difficult to define, since the meaning of the angle β changes after the transition state when the bond is broken. The fact that the dihedral angle γ approaches a constant value of zero at the transition state suggests that the nitrogen is also close to sp^2 hybridized at this point.

These observations are consistent with an orbital picture that places the unpaired electron of the reactant radical in an orbital centered on carbon, which is between sp^3 and p in character. The nitrogen bears three bonding pairs of electrons ($N-H$, $N-C$, and $N-O$) and a lone pair. As the reaction progresses, the carbon-centered atomic orbital containing the unpaired electron and the $N-O$ σ orbital are converted smoothly into the $C-N$ π orbital and an atomic one-electron orbital centered on oxygen. The MCSCF calculations provide an electronic energy barrier of 2.49 kcal/mol, which is corrected to 0.07 kcal/mol by MRMP2.

Lower level calculations on the model compound were performed in the same manner using the semiempirical UPM3 method,[14] the ROHF method, and Becke's three-parameter hybrid density-functional with Perdew and Wang's 1991 exchange-correlation functional, B3PW91.[1,15]

(12) (a) Ditchfield, R.; Hehre, W. R.; Pople, J. A. *J. Chem. Phys.* **1971**, *54*, 724. (b) Hehre, W. R.; Ditchfield, R.; Pople, J. A. *J. Chem. Phys.* **1972**, *56*, 2257. (c) Hariharan, P. C.; Pople, J. A. *Theor. Chim. Acta* **1973**, *28*, 213. (d) Clark, T.; Chandrasekhar, J.; Spitznagel, G. W.; Schleyer, P. von R. *J. Comput. Chem.* **1983**, *4*, 294.

(13) (a) Corresponding extensive pyramidalization at carbon is not observed in the pyridyl radicals because of delocalization. (b) The pyramidalization of **1** is comparable to that observed in simple α-amino radicals.[13c,d] (c) Armstrong, D. A.; Rauk, A.; Yu, D. *J. Am. Chem. Soc.* **1993**, *115*, 666. (d) Wayner, D. D. M.; Clark, K. B.; Rauk, A.; Yu, D.; Armstrong, D. A. *J. Am. Chem. Soc.* **1997**, *119*, 8925.

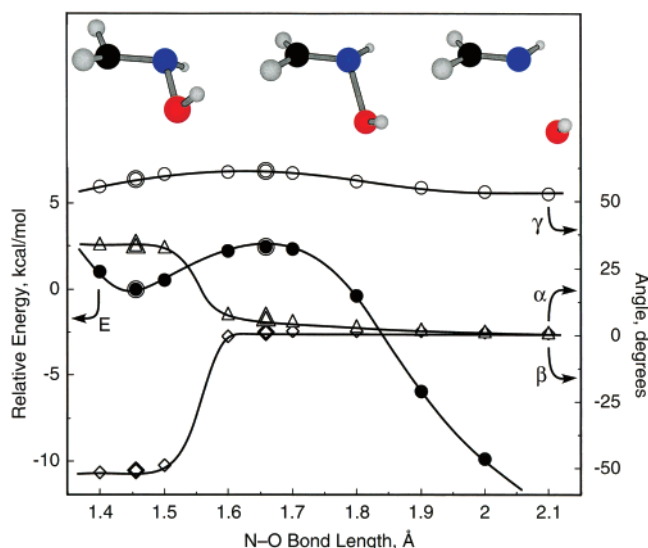(14) Stewart, J. J. P. *Rev. Comput. Chem.* **1990**, *1*, 45.

FIGURE 1. Left scale, CASSCF(25,15)/6-31+G* energies *E* (filled circles) of radical **1**, as a function of N−O bond length, and normalized to zero at the radical minimum structure. Right scale, the angles α (open triangles), β (open diamonds), and γ (open circles), as defined in Scheme 1, as a function of N−O bond length, showing flattening at both carbon and nitrogen as the reaction proceeds. The positions of the radical minimum and the reaction transition state are indicated by the outlined symbols. Also shown are the MCSCF/6-31+G* calculated structures of the radical at the minimum (N−O = 1.46 Å), at the transition state (N−O = 1.66 Å), and at an N−O bond distance of 2.1 Å, a point substantially past the transition state.

This method was chosen since hybrid methods have been shown to describe bond cleavage more accurately than pure DFT methods.[16] The results are summarized in Figure 2.

The ROHF method was expected to provide an approximate picture of the fragmentation reaction *in the absence* of state mixing, since the formalism of ROHF prevents the required spin interaction. The other methods all include this mixing (configuration interaction) to differing degrees of accuracy and, thus, should give energies that are lower that the ROHF energies, at least in the region of the transition state. That this is true is easily observed in Figure 2, which shows that ROHF hugely overestimates the reaction barrier, as expected. PM3 apparently does a better job of describing the reaction energetics but is plagued by spin contamination, which may be responsible for the minimum near 1.9 Å.

Of the lower level methods, Figure 2 clearly shows that the DFT energies as a function of N−O bond length are in good agreement with those from MCSCF, especially up to their respective transition states. At large N−O bond lengths, however, the DFT and MCSCF results are substantially different, with the DFT energies being higher than expected. This is presumably due to a difference in the size-extensivity of the two methods.[17]

(15) (a) Becke, A. D. *J. Chem. Phys.* **1993**, *98*, 5648. (b) Hehre, W. J.; Ditchfield, R.; Pople, J. A. *J. Chem. Phys.* **1972**, *56*, 2257. (c) Krishnan, R.; Binkley, J. S.; Seeger, R.; Pople, J. A. *J. Chem. Phys.* **1980**, *72*, 650. (d) McLean, A. D.; Chandler, G. S. *J. Chem. Phys.* **1980**, *72*, 5639.

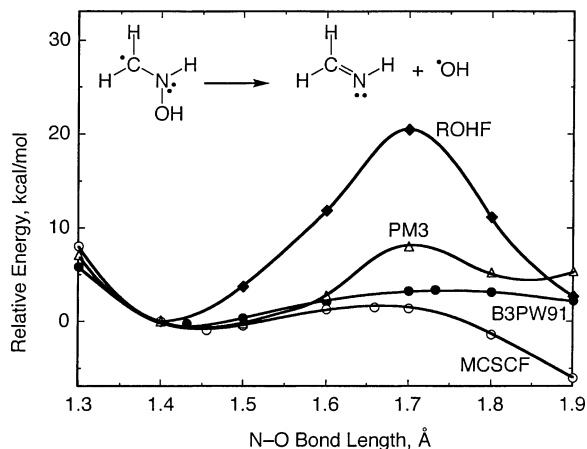(16) Jensen, F. *Introduction to Computational Chemistry*; Wiley: New York, 1999; p 283.

FIGURE 2. Relative energies as a function of N−O bond stretching for radical **1** computed using various methods indicated in the figure, i.e., open circles, MCSCF/6-31+G*; closed circles, B3PW91/6-31+G*; triangles, PM3; closed diamonds, ROHF/6-31+G*. The energies are purely electronic for the DFT and ab initio methods. All energies are normalized to zero at an N−O bond length of 1.4 Å.

Fortunately, this is not an issue for the current study, in which only the potential surface up to the transition state is of concern. The transition state has a slightly longer N−O bond length using ROHF, UPM3, or DFT compared to that given by MCSCF.

The DFT radical minimum is at a slightly shorter N−O bond length (1.43 Å) than the MCSCF (1.46 Å), but otherwise, the structures are similar. The transition states are less so, however. The potential energy surfaces near the transition state are fairly flat along the reaction coordinate; thus, it is not surprising that there is some variation in its location. DFT places the transition state somewhat farther along the reaction coordinate (1.73 Å versus 1.66 Å for MSCCF) and at a slightly higher energy (3.59 kcal/mol).

Comparison of DFT Barriers with Experiment. DFT calculations were performed on the pyridyl radicals summarized in Table 1, for which experimental reaction barriers have previously been determined. Calculations were again performed as constrained geometry optimizations at regular N−O bond length intervals and as unconstrained optimizations of the radical minima and reaction transition states. The minima and transition states were characterized by post-optimization frequency calculations. Selected geometric information and the electronic energy differences between radical minimum and transition state for each radical are summarized in Table 1. Potential energy curves for the various reactions are illustrated in Figure 3.

As for the model, the radicals of Table 1 are pyramidalized both at their minimum geometries and at their transition states. Pyramidalization in this case is most easily characterized by the O−N−p-C bond angle, δ, eq 4. Three trends are noticeable in the data of Table 1.

$$(4)$$
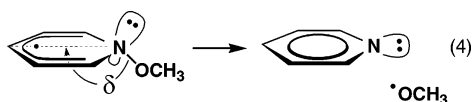
There are correlations between the barrier height and

TABLE 1. Relative Electronic Energies and Geometric Parameters for the Minimum and Transition State Structures for Fragmentation of the N−O Bond in *N*-Methoxypyridyl Radicals, Calculated Using B3PW91/6-31+G*

Structure	Radical	$\Delta E^{\ddagger}_{DFT}$ [a] (kcal/mol)	r_{N-O}^{min} [b] (Å)	δ^{min} [c] (°)	$r_{N-O}^{\ddagger}$ [b] (Å)	$\delta^{\ddagger}$ [c] (°)
MeO-N⁺⟨⟩⟨⟩N-OCH₃	2	19.99	1.373	175.2	1.825	133.2
O₂N⟨⟩N-OCH₃	3	9.08	1.377	175.0	1.715	134.3
⟨⟩=⟨⟩N-OCH₃	4	4.09	1.408	153.8	1.665	132.0
NC⟨⟩N-OCH₃	5	4.51	1.405	154.6	1.667	133.1
⟨⟩⟨⟩N-OCH₃	6	1.58	1.428	147.2	1.612	133.0
⟨⟩⟨⟩N-OCH₃	7	0.35	1.457	141.6	1.568	134.2
⟨⟩N-OCH₃	8	0.43	1.457	141.2	1.575	133.7
MeO-⟨⟩N-OCH₃	9	-1.28 [d]	1.45 [d]	136.5 [d]	1.55 [d]	130.9 [d]

[a] Electronic energy of the transition state minus that of the minimum. [b] Calculated N−O bond distance at the radical minimum and transition state. [c] Calculated angle δ (see eq 3) at the radical minimum and transition state. [d] These values refer to an average of those computed at 1.4 and 1.5 Å for the minimum and 1.5 and 1.6 Å for the transition state, since no barrier was found in this case. These points on the potential energy surface were chosen on the basis of data from the fastest compound which was determined to have a barrier.
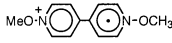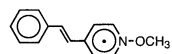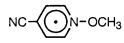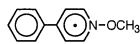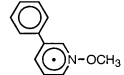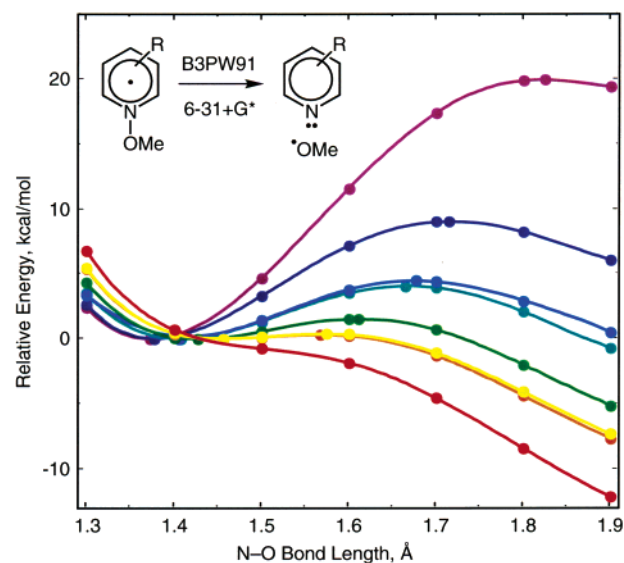

FIGURE 3. Electronic energies as a function of the N−O bond length, computed using the B3PW91/6-31+G* method, and normalized to zero at 1.4 Å, for (in order from top to bottom at right edge of the graph) *N*-methoxypyridyl radicals **2−9** (see Table 1 for structures).

the N−O bond length at the radical minima, the pyramidalization angle δ at the radical minima, and the N−O bond length at the transition state. The pyramidalization

(17) Jensen, F. *Introduction to Computational Chemistry*; Wiley: New York, 1999; pp 189, 117.

TABLE 2. Calculated (B3PW91/6-31+G*) and Experimental Kinetic Parameters for N−O Bond Fragmentation in *N*-Methoxypyridyl Radicals

Structure	Radical	$\Delta G^{\ddagger}_{DFT}$ [a]	k_{DFT} [a]	k_{Exp} [b]	$\Delta G^{\ddagger}_{Exp}$ [b]
		(kcal/mol)	(s⁻¹)	(s⁻¹)	(kcal/mol)
	2	18.51[c]	1.6 x 10¹[c]	4.0 x 10⁴	11.2
		14.38[d]	1.8 x 10²[d]		
	4	2.71	6.4 x 10¹⁰	4.6 x 10⁹	4.3
	5	3.10	3.3 x 10¹⁰	1.2 x 10¹⁰	3.7
	6	0.70	1.9 x 10¹²	2.7 x 10¹¹	1.9
	7	-0.22	9.0 x 10¹²	8.3 x 10¹¹	1.2
	8	-0.22	9.1 x 10¹²	1.6 x 10¹²	0.8

[a] Calculated (B3PW91/6-31+G*) reaction free energy barrier and rate constant (see text). [b] Experimental reaction free energy barrier and rate constant (see ref 5 and text). [c] DFT calculations without solvent correction (see text). [d] DFT calculations with solvent correction (see text).
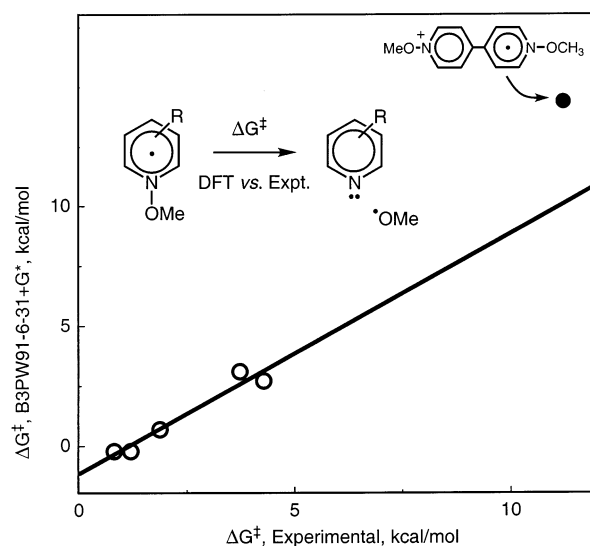

FIGURE 4. Plot of calculated (B3PW91/6-31+G*) versus experimental free energy of activation for N−O bond fragmentation in *N*-methoxypyridyl radicals **3**−**7** (open circles, see Table 2). The straight line has a slope of 1.0 and an intercept of −1.2 kcal/mol and shows that the calculated values are on average ca. 1 kcal/mol smaller than experiment but that the overall correlation is excellent. The filled circle is for the charged radical **2** (indicated, see Table 2) and is off the line for the reasons discussed in the text.

angles at the minima vary significantly, increasing from 175° to ca. 141° as the electronic barrier decreases from 19.99 to 0.43 kcal/mol. In fact, the only parameter that does not seem to vary significantly is the angle δ at the transition state (mean: 133.4° ± 0.8°). This suggests that the prerequisite amount of $\sigma^*-\pi^*$ mixing at the transition state is independent of the substituent and that one of the main factors controlling the rate constant is the extent to which this mixing is lacking in the geometry of the radical minimum. The closer the geometry of the radical is to that of the transition state, the lower the barrier. The N−O bond lengths in the radical minima exhibit the same trend, with increasing bond length in the minimum configuration corresponding to faster reaction. Obviously, increasing the extent of $\sigma^*-\pi^*$ mixing increases the length of the N−O bond at the minimum.

As discussed above,[5,7] differing extents of mixing correspond to differing extents of N−O bending; indeed, this mixing is the main factor that is responsible for the bending both at the minimum and also at the transition state. Electron-withdrawing and delocalizing groups decrease the $\sigma^*-\pi^*$ mixing, which favors a more planar geometry and a stronger N−O bond. Electron-donating groups increase the mixing, favoring a more bent geometry, weakening the N−O bond and increasing its length.

The calculated free energy barriers for the reactions ($\Delta G^{\ddagger}_{DFT}$, given by the free energy difference between the minimum and transition state geometries) are summarized in Table 2, together with corresponding rate constants (k_{DFT}) calculated using the Eyring transition state theory equation, eq 5a. Also given in Table 2 are the experimental reaction rate constants (k_{Exp}) in acetonitrile solvent and corresponding experimental reaction free energies, $\Delta G^{\ddagger}_{Exp}$, obtained again using the Eyring transition-state theory equation, eq 5b.

$$k_{DFT} = \frac{kT}{h} e^{-\Delta G^{\ddagger}_{DFT}/RT} \tag{5a}$$

$$\Delta G^{\ddagger}_{Exp} = RT\left(\ln \frac{kT}{h} - \ln k_{Exp}\right) \tag{5b}$$

Equating the $\Delta G^{\ddagger}_{DFT}$ with transition-state theory reaction barriers $\Delta G^{\ddagger}_{Exp}$ allows a direct comparison with experiment. A plot of $\Delta G^{\ddagger}_{DFT}$ versus $\Delta G^{\ddagger}_{Exp}$ is given in Figure 4, together with a linear fit to the data, with the point for the bipyridinium radical cation **2** excluded, for reasons discussed below. The slope of the fitted line is 1.0, with an intercept just below zero (−1.2), over a range of free energies of ca. 3.5 kcal/mol, corresponding to a range of rate constants of almost 3 orders of magnitude. Inspection of Table 2 shows that the calculated and experimental values are within ca. 3 kcal/mol of each other for a range of rate constants of 8 orders of magnitude. Clearly, the DFT and the experimental activation free energies agree quite well. The DFT barriers are uniformly smaller that the experimental barriers by ca. 1 kcal/mol. The fact that DFT gives reaction barriers that are somewhat lower than expected has been discussed previously,[18] although the differences in this case are small.

An important factor favoring a good correlation between the experimental and theoretical free energy barriers is that the reactions are of neutral radicals fragmenting to give neutral products. No strong solvent effect is expected in this case, allowing a closer cor-

(18) Lynch, B. J.; Fast, P. L.; Harris, M.; Truhlar, D. G. *J. Phys. Chem. A* **2000**, *104*, 4811.

respondence of solution-phase experiments and gas-phase calculations. The radical with the poorest agreement is the charged radical **2**. In the radical, the charge is evenly delocalized over the two nitrogens as a consequence of the symmetry of the structure. In the heterocycle formed after cleavage, the charge will be localized on the remaining quaternary nitrogen. Thus, the charge localizes as the cleavage reaction proceeds. A polar solvent should lower the energy of the transition state more than that of the starting radical, and the experimental barrier should be smaller than the gas-phase calculated barrier, as was observed.

This solvent effect for radical **2** was investigated computationally. Estimates of solvation energy were made using the PCM model of acetonitrile as implemented in Gaussian 98.[19] A large solvation energy for the cation radical **2** of 34.8 kcal/mol was found, while the similar but uncharged radical **6** exhibited a small solvation energy, 3.4 kcal/mol. More importantly, solvation at the minimum for **2** was smaller than for the transition state, resulting in a substantial reduction in the computed barrier height in acetonitrile, from 18.5 to 14.4 kcal/mol, Table 2. The corresponding computed solvent effect on the barrier for the uncharged radical **6** was negligible, 0.25 kcal/mol. Although the computed barrier is still larger than the experimental barrier, this indicates that solvent effects are responsible for the difference in this case.

The DFT results of Figure 3 follow the predictions of the qualitative model described previously.[5] The barrier increases with electron-withdrawing and/or -delocalizing substituents. The barrier decreases with the addition of an electron-donating *p*-methoxy group, **8**, to the extent that both the free energy and electronic barriers to reaction disappear, Figure 3. Even taking into account the fact that the DFT free energies are smaller that the actual values, the potential energy surface for **8** exhibits no minimum close to any expected radical minimum geometry. Note that the energy curve is not purely dissociative; the attractive part of the potential remains visible. A plot of the derivative of the energy curve for this radical yields a single maximum, where the slope is closer to zero than at any other point. Even here, the slope is slightly more than 5 kcal/mol·Å, indicating that at no point does the potential energy surface even approach being horizontal. Together with the experimental observation of no detectable radical intermediate, this provides theoretical support for the suggestion of an essentially barrierless reaction in this case.[5b]

Finally, it is worth mentioning that the DFT method reproduces the experimental barriers in these reactions well even though the reactions involve extensive mixing of π^* and σ^* states. As discussed in detail elsewhere, the energy splitting along the reaction path between the ground and excited states formed as a result of this mixing is quite large, being >30 kcal/mol for most of the reactions.[20] Nevertheless, the character of the reacting state must change smoothly, increasing in σ^* character along the reaction coordinate. The configuration interac-

tion responsible for this change in electronic character is evidently accounted for quite well in the B3PW91 method.[21]

Conclusions

For the solution-phase N—O bond cleavage reaction of a series of *N*-methoxyheterocyclic radicals, B3PW91/6-31+G* electronic structure calculations reproduce the experimental free energy barriers within ca. 1 kcal/mol over a range of rate constants spanning 3 orders of magnitude and are within ca. 3 kcal/mol over 8 orders of magnitude in rate constant. The DFT calculations also agree well with MCSCF calculations for a model radical reaction. These data provide support for the applicability of DFT calculations to reactions of this type. The calculations also provide further support for a truly barrierless fragmentation reaction in this series.

Experimental Section

The DFT calculations were performed with Gaussian 98 on a personal computer running Windows[22] or on an NCSA (University of Illinois, Urbana—Champaign) supercomputer.[23] All GAMESS calculations were performed on a Silicon Graphics Origins 2000 8-processor mainframe.[24]

For the FORS-type MCSCF calculations on the model radical **1**, an all-electron active space [CASSCF(15/25)] was required to overcome active space instabilities. Since using a smaller active space can cause incorrect results, but a larger active space should either have no effect or should only increase accuracy (so long as no superfluous orbital is significantly excited), the large active space should not cause any problems. The determinant configuration interaction scheme developed in the Ames laboratory for GAMESS was employed in every case, and every possible spin-allowed excitation was considered in the MCSCF calculation (full active space CI). The MCQDPT2 method implemented in GAMESS was used to find the single-point perturbationally corrected energy. The

(21) For a discussion, see: Jensen, F. *Introduction to Computational Chemistry*; Wiley: New York, 1999; pp 283, 284.

(22) Gaussian 98W, Revision A.7: Frisch, M. J.; Trucks, G. W.; Schlegel, H. B.; Scuseria, G. E.; Robb, M. A.; Cheeseman, J. R.; Zakrzewski, V. G.; Montgomery, J. A., Jr.; Stratmann, R. E.; Burant, J. C.; Dapprich, S.; Millam, J. M.; Daniels, A. D.; Kudin, K. N.; Strain, M. C.; Farkas, O.; Tomasi, J.; Barone, V.; Cossi, M.; Cammi, R.; Mennucci, B.; Pomelli, C.; Adamo, C.; Clifford, S.; Ochterski, J.; Petersson, G. A.; Ayala, P. Y.; Cui, Q.; Morokuma, K.; Malick, D. K.; Rabuck, A. D.; Raghavachari, K.; Foresman, J. B.; Cioslowski, J.; Ortiz, J. V.; Baboul, A. G.; Stefanov, B. B.; Liu, G.; Liashenko, A.; Piskorz, P.; Komaromi, I.; Gomperts, R.; Martin, R. L.; Fox, D. J.; Keith, T.; Al-Laham, M. A.; Peng, C. Y.; Nanayakkara, A.; Gonzalez, C.; Challacombe, M.; Gill, P. M. W.; Johnson, B.; Chen, W.; Wong, M. W.; Andres, J. L.; Gonzalez, C.; Head-Gordon, M.; Replogle, E. S.; Pople, J. A. Gaussian, Inc., Pittsburgh, PA, 1998.

(23) Gaussian 98, Revision A.11.3: Frisch, M. J.; Trucks, G. W.; Schlegel, H. B.; Scuseria, G. E.; Robb, M. A.; Cheeseman, J. R.; Zakrzewski, V. G.; Montgomery, J. A., Jr.; Stratmann, R. E.; Burant, J. C.; Dapprich, S.; Millam, J. M.; Daniels, A. D.; Kudin, K. N.; Strain, M. C.; Farkas, O.; Tomasi, J.; Barone, V.; Cossi, M.; Cammi, R.; Mennucci, B.; Pomelli, C.; Adamo, C.; Clifford, S.; Ochterski, J.; Petersson, G. A.; Ayala, P. Y.; Cui, Q.; Morokuma, K.; Rega, N.; Salvador, P.; Dannenberg, J. J.; Malick, D. K.; Rabuck, A. D.; Raghavachari, K.; Foresman, J. B.; Cioslowski, J.; Ortiz, J. V.; Baboul, A. G.; Stefanov, B. B.; Liu, G.; Liashenko, A.; Piskorz, P.; Komaromi, I.; Gomperts, R.; Martin, R. L.; Fox, D. J.; Keith, T.; Al-Laham, M. A.; Peng, C. Y.; Nanayakkara, A.; Challacombe, M.; Gill, P. M. W.; Johnson, B.; Chen, W.; Wong, M. W.; Andres, J. L.; Gonzalez, C.; Head-Gordon, M.; Replogle, E. S.; Pople, J. A. Gaussian, Inc., Pittsburgh, PA, 2002.

(24) GAMESS Version 26 OCT 2000: Schmidt, M. W.; Baldridge, K. K.; Boatz, J. A.; Elbert, S. T.; Gordon, M. S.; Jensen, J. H.; Koseki, S.; Matsunaga, N.; Nguyen, K. A.; Su, S. J.; Windus, T. L.; Dupuis, M.; Montgomery, J. A. *J. Comput. Chem.* **1993**, *14*, 1347−1363.

(19) Barone, V.; Cossi, M.; Tomasi, J. *J. Chem. Phys.* **1997**, *107*, 3210.

(20) Lorance, E. D.; Gould, I. R. *J. Phys. Chem. A*, submitted.

nature of each stationary point was verified by frequency calculations.

Single-point energy corrections were calculated using the PCM-SCRF method as implemented in Gaussian 98, using the United Atom Topological Model to construct the cavity and requesting 80-facet polyhedra. The solvent correction to the electronic energy was used in conjunction with the gas-phase thermodynamic data to estimate a solvated free energy for radicals **2** and **6**.

Supporting Information Available: Tables SI-1−5. This material is available free of charge via the Internet at http://pubs.acs.org.

JO040259Q